HHS Public Access

Author manuscript

J Neural Eng. Author manuscript; available in PMC 2017 August 01.

Published in final edited form as:

J Neural Eng. 2016 August ; 13(4): 046019. doi:10.1088/1741-2560/13/4/046019.

Histological Evaluation of a Chronically-implanted Electrocorticographic Electrode Grid in a Non-human Primate

Alan D. Degenhart[1,2,4,*], **James Eles**[1,2,*], **Richard Dum**[2,4], **Jessica L. Mischel**[1,2], **Ivan Smalianchuk**[1,2], **Bridget Endler**[1,2], **Robin C. Ashmore**[3], **Elizabeth C. Tyler-Kabara**[1,3,5,9], **Nicholas G. Hatsopoulos**[6,7], **Wei Wang**[1,2,3,8,^], **Aaron P. Batista**[1,2,4,^], and **X. Tracy Cui**[1,2,9,^]

[1]Department of Bioengineering, University of Pittsburgh, Pittsburgh, PA

[2]Center for the Neural Basis of Cognition, Pittsburgh, PA

[3]Department of Physical Medicine and Rehabilitation, University of Pittsburgh, School of Medicine, Pittsburgh, PA

[4]Systems Neuroscience Institute, University of Pittsburgh School of Medicine, Pittsburgh, PA

[5]Department of Neurological Surgery, University of Pittsburgh, Pittsburgh, PA

[6]Department of Organismal Biology and Anatomy, University of Chicago, Chicago, IL

[7]Committee on Computational Neuroscience, University of Chicago, Chicago, IL

[8]Clinical and Translational Science Institute, University of Pittsburgh, Pittsburgh, PA

[9]McGowan Institute for Regenerative Medicine, Pittsburgh, PA

Abstract

Electrocorticography (ECoG), used as a neural recording modality for brain-machine interfaces (BMIs), potentially allows for field potentials to be recorded from the surface of the cerebral cortex for long durations without suffering the host-tissue reaction to the extent that it is common with intracortical microelectrodes. Though the stability of signals obtained from chronically-implanted ECoG electrodes has begun receiving attention, to date little work has characterized the effects of long-term implantation of ECoG electrodes on underlying cortical tissue. We implanted a high-density ECoG electrode grid subdurally over cortical motor areas of a Rhesus macaque for 666 days. Histological analysis revealed minimal damage to the cortex underneath the implant, though the grid itself was encapsulated in collagenous tissue. We observed macrophages and foreign body giant cells at the tissue-array interface, indicative of a stereotypical foreign body response. Despite this encapsulation, cortical modulation during reaching movements was observed more than 18 months post-implantation. These results suggest that ECoG may provide a means by which stable chronic cortical recordings can be obtained with comparatively little tissue damage, facilitating the development of clinically-viable brain-machine interface systems.

*Denotes equal contributions.

^Denotes co-corresponding authors. xic11@pitt.edu, bmewang@gmail.com, apb10@pitt.edu

1. Introduction

Brain-machine interfaces (BMIs) utilize cortical signals to directly control external devices for restoration of motor function in individuals with disabilities (Moran, 2010; Schwartz et al., 2006; Wolpaw et al., 2002; Leuthardt et al., 2006). A critical component of a BMI system is the neural recording modality used to extract meaningful information from the brain. The primary modalities used in clinical BMI systems are electroencephalography, electrocorticography (ECoG), local field potentials, and single/multi-unit activity. These methods can be characterized by factors such as performance, decoding stability, longevity, and invasiveness. The choice of a neural recording modality for a particular BMI application must appropriately weigh these factors.

Penetrating intracortical electrode arrays offer the highest spatial and temporal resolution in neural recording. However, the implantation of these arrays disrupts brain tissue and vasculature, and leads to a chronic inflammatory response hallmarked by an aggregation of astrocytes and microglia in a glial scar around the probe, as well as progressive neuronal degeneration at the vicinity of the implanted electrodes (Polikov et al., 2005; McConnell et al., 2009; Biran et al., 2005). This ultimately leads to recorded signal deterioration, manifested as a reduction in the number of electrodes recording individual neurons or a decrease in signal amplitude (Barrese et al., 2013; Schwartz et al., 2006; Moran, 2010; Freire et al., 2011; Collinger et al., 2012; Schwartz, 2004; Simeral et al., 2011; Chestek et al., 2011). Further, meningeal tissue proliferation and fibrous encapsulation have the potential to dislodge the implanted intracortical devices (Barrese et al., 2013).

ECoG is a recording modality where electrodes are placed either subdurally (below the dura) or epidurally (on the surface of the dura) to record electrical field potentials generated by aggregate cortical activity. Since ECoG arrays do not penetrate the cortex, they avoid blood-brain barrier disruption and mechanical strain between the brittle electrode and soft neural tissue, which are common for intracortical electrodes. This potentially mitigates some inflammatory burden on the brain. ECoG signals have been found to encode information about arm and hand movements (Leuthardt et al., 2004; Schalk et al., 2007; Crone et al., 1998; Miller et al., 2007; Pistohl et al., 2008; Wang et al., 2009; Kubánek et al., 2009; Ball et al., 2009; Miller et al., 2009; Chao et al., 2010; Acharya et al., 2010; Degenhart et al., 2011a; Shimoda et al., 2012; Chestek et al., 2013; Nakanishi et al., 2013), as well as auditory (Edwards et al., 2005; Trautner et al., 2006), visual (Lachaux et al., 2005), language (Crone et al., 2001; Mainy et al., 2007; Kellis et al., 2010; Wang et al.; 2011, Pei et al., 2011), and attentional processes (Tallon-Baudry et al., 2005; Jung et al., 2008; Ray et al., 2008). Encouraged by these findings, researchers have begun to investigate ECoG as a potential source of control signals for BMI devices. Human and non-human primate subjects have demonstrated up to three-dimensional control of computer cursors or prosthetic limbs using ECoG (Leuthardt et al., 2011; Schalk and Leuthardt, 2011; Leuthardt et al., 2004; Schalk et al., 2008; Wilson et al., 2006; Yanagisawa et al., 2012; Wang et al., 2013; Hotson et al., 2016).

Despite the promise of ECoG in BMI and neuroscience applications, very few studies have evaluated the long-term host-tissue response to either epidural or subdural grids. In humans

and non-human primates, subdural and epidural arrays have been implanted for over one year with viable neural recording, however these studies did not report end-term tissue health (Shimoda et al., 2012; Morrell and RNS System in Epilepsy Study Group, 2011). Additionally, electrode grids are frequently implanted subdurally for up to 30 days in humans for purposes of epilepsy monitoring. While limited incidents of bleeding, infection, infarction, and functional deficits have been reported in association with these implants, no macroscopic fibrotic growth has been reported in otherwise uncomplicated surgeries (Fountas and Smith, 2007; Van Gompel et al., 2008; Wong et al., 2009). Some longer-term studies (> 1 year) of subdural spinal and cortical stimulators and probes reported encapsulation or dural thickening in the vicinity of the implants (Nashold and Friedman, 1972; Pineda, 1978; Saitoh et al., 2000; Sillay et al., 2013). In rats, just one week after an epidural implantation, connective tissue overgrowth was observed (Schendel et al., 2014; Schendel et al., 2013). These studies followed tissue growth around epidural ECoG grids implanted in rats for up to 419 days, showing dural thickening under the arrays and tissue encapsulation over the top of the array as early as one month following implantation. (Schendel et al., 2014). These findings are corroborated by findings of dural thickening at 6 months post subdural implant. Tissue proliferation was correlated with a rise in 1kHz electrical impedance as early as 1 week, with stabilization at 18 weeks post-implant (Henle et al., 2011). This would presumably reduce the quality of any neural signal recorded by the ECoG array, though no study has correlated long-term tissue reaction with neural signal quality. While Schendel et al. and Henle et al. investigated possible glial reaction to epidural and subdural implantation in the superficial layers of cortex, few studies explore the impact of subdural grids on deeper layers of the cortical tissue, particularly on neuronal health.

The current study explores the host-tissue response to a subdural ECoG grid implanted for 666 days, focusing on both cortical tissue health and fibrosis at the implant site, while also validating device performance by examining neural responses to overt reaching movements. We found that cortical thickness and neuronal density was unaffected by array implantation. Furthermore, while microglial density was increased in superficial cortical layers, they were in a resting stage morphology, and astrocyte activation was consistent with tissue not under the implant. Finally, though the grid itself was found to be encapsulated in a fibrous envelope upon explantation, robust modulation of ECoG signals was observed over 18 months post-implantation.

2. Methods

All experimental procedures were approved by the Institutional Animal Care and Use Committee of the University of Pittsburgh and were in accordance with the National Institutes of Health's Guidelines for the Care and Use of Laboratory Animals.

2.1. ECoG grid implantation surgery

An adult male Rhesus monkey (*macaca mulatta*) was anesthetized, and a craniotomy was performed to expose the left motor and premotor cortex. The dura was retracted to expose an area approximately 2×2 cm between the arcuate and central sulci. A custom-built 15-channel, 1 mm thick silicone ECoG grid with 2mm diameter platinum electrode sites (Figure

1A, PMT Corp, Chanhassen, MN, USA), identical in construction to FDA-approved electrode grids commonly used for epilepsy monitoring, was placed directly on the exposed brain surface (Figure 1B–C). After positionin, the dura and the bone were reapproximated. Wires from the grid were connected to a Cereport pedestal connector (Blackrock Microsystems, Salt Lake City, UT, USA) affixed to the skull.

2.2. Neural recording and task control

Signals from the ECoG grid were recorded with a g.USBamp Biosignal Amplifier (g.tec Medical Engineering) and sampled at 1200 Hz. All recording, online processing, task control and presentation was performed using the Craniux Brain Computer Interface system (Degenhart et al., 2011b). Dura-facing electrodes 4 and 13 were used as reference and ground electrodes, respectively, for all recordings (Figure 1A). Visual stimuli were presented on a 22-inch computer monitor placed approximately 0.8 meters from the monkey.

2.3. Hand control task

In order to validate device performance and ECoG signal modulation at long-term time points, we analyzed data recorded approximately 18 months post-implantation (day 542 to day 562 post-implant). During these experiments, the animal performed a standard 2D center-out task in a virtual environment, with the position of the hand controlling the location of a computer cursor in a two-dimensional frontoparallel plane. Hand position was tracked in real-time using an optical tracking system (Phasespace, San Leandro, CA) and rendered on a computer screen as a sphere in a virtual workspace. Trials began with the appearance of the cursor and central target; the animal was then required to move the cursor to the central target, and hold it there for 400–600 ms. One of eight peripheral targets would then appear, to which the animal was required to reach. A target hold time of 200 ms was enforced. The animal was provided a water reward immediately following successful completion of a trial.

Prior to offline analysis, hand control trials were visually examined for artifacts in both the time and time-frequency domains; all trials exhibiting artifacts during the central hold or target acquisition periods were excluded from further analysis. These artifacts were characterized by large-amplitude, broadband transients across the majority of recording electrodes, and are believed to be the result of jaw movements based on their consistent appearance during the reward period of each trial. Time domain data from the remaining trials were transformed into the time-frequency domain using the Burg autoregressive method (0 – 200Hz range, 2Hz frequency bands, 100th order, 100ms non-causal window, 33ms step size), log-transformed, then normalized to pseudo Z-scores relative to the spectral power during the central target hold period. Trials were then manually aligned to movement onset using the cursor speed profile for each trial.

2.4. Explant

Electrodes remained implanted for a total of 666 days, after which the animal was sacrificed and the electrode grid removed. Surgical complications unrelated to the ECoG grid negated the possibility of perfusing the animal before removing the brain. After exposure of the skull, the original bone flap was removed to expose the dura. The skull proximal to the

connector, the dura, and the encapsulated electrode grid were then removed as a single piece and the entire brain was extracted. The brain and the encapsulated array were then placed in a 10% formalin + 10% glycerin solution for 8 days followed by 10% formalin + 20% glycerin for 26 days to fixate the tissue. The brain was bisected along the midline and 3D renderings of each hemisphere were generated with a 3D scanner (Faro Platinum Arm, Faro, Warwickshire, UK). Surface topography of the implanted hemisphere was quantitatively compared to the mirror image of the non-implanted hemisphere using Geomagic Studio (Geomagic. Rock Hill, SC). Fixated tissue was then frozen and sectioned into 50μm sections for staining. Sections were cut perpendicular to the central sulcus. The electrode grid was carefully removed from the encapsulation "envelope," which was similarly fixed for 26 days and then stored in phosphate tris azide (PTA) solution until it was cut into 50μm sections for staining. Encapsulation tissue was cut perpendicular to the placement of the grid.

2.5. Immunohistochemistry

Cortical sections from implanted (left) and non-implanted (control, right) hemispheres were mounted on the same slide for comparison, and all slides were processed in the same session to minimize variability. A sample of dura mater distant from the edges of the tissue encapsulation (> 2cm) served as control dura mater for analysis of the encapsulation tissue.

Antibodies for cortical tissue were directed to neurons (NeuN, 1:200, Millipore), astrocytes (GFAP, 1:200, SeroTec), or microglia (Iba-1, 1:500, Fisher); antibodies for encapsulation/dura mater tissue were directed to macrophages (Iba-1, 1:500, Fisher) or fibroblasts/macrophages (Vimentin, 1:250, Millipore). Tissue was first blocked for 30 minutes in sodium citrate buffer (0.1M citric acid, 0.1M sodium citrate, pH 6.0) in room temperature followed by a peroxidase block (10% methanol, 3% hydrogen peroxide) for 20 minutes in room temperature on a shaker. Then, tissue was blocked in a serum containing blocking buffer (5% normal goat serum, Jackson Labs; 0.1% Triton X-100, Sigma) for one hour. Tissue was incubated in primary antibody for 12–24 hours. Following washes in phosphate buffer saline (PBS), tissue was incubated in 1:250 Alexa Fluor 488 and/or 633 (Invitrogen) for 2 hours at room temperature, followed by more PBS washes, 10 minute incubation in Hoescht 33342 (1uL/1mL; Invitrogen) stain, and more PBS washes. Coverslips were then mounted with Fluoromount-G (Southern-Biotech).

2.6. Confocal imaging

All confocal imaging was performed with an Olympus Fluoview 1000 confocal scanning microscope (Olympus Corporation, Tokyo, Japan). All images were taken with a 20× or 40× objective to optimize cellular resolution and image frame size. Images were taken at multiple focal depths for each frame in order to image the full depth of a tissue slice. This ensured that image analysis was not biased by choice of a single image depth. Confocal laser power, photomultiplier tube voltage (the sensitivity of the image detector), and photomultiplier offset (background level of image detector) were selected to ensure that image pixels did not exceed upper or lower detection limits. Images (n = 5 tissue sections per stain) were collected from cortical regions directly under electrode sites in Brodmann Area 4 (specific sites denoted by blue circles in Figure 1E) on the ECoG array or from the thickest region of both the dorsal and ventral sides of the center of the tissue encapsulation.

Images collected were only excluded from analysis on grounds of poor quality of signal, photobleaching, or severe tissue tears during processing. For cortical tissue imaging, images from the contralateral hemisphere were collected for comparison. Images were matched to the same sagittal slice depth and anterior-posterior region of interest as the ipsilateral hemisphere. Tissue encapsulation images were compared to images from random regions of interest of control dura mater retrieved from > 2cm from the tissue encapsulation.

To determine cortical layers and cortical thickness, disconnected images of cortex were stitched to create continuous high-resolution images of the entire cortical depth using Fiji, an Image-J (NIH) plug-in (Preibisch et al., 2009). Layers I/II–III were discerned from layer V by the location of layer V giant pyramidal cells (Matelli et al., 1991). Stitched images were used to measure cortical depth (n = 5) between conditions. Neuronal and microglial cell densities were determined for layers I/II–III and V with manual counting facilitated by Image J Cell Counter (n = 5). Layer I microglia morphology was assessed as previously described (Stence et al., 2001; Nimmerjahn et al., 2005; Kozai et al., 2012). Microglia were deemed to be 'unresponsive' if they were ramified (resting) or activated but not extending processes to the cortical surface, and 'surface directed' if they had activated or amoeboid morphology, with processes extended to or along the cortical surface. Because GFAP labels extensive networks of astrocytic processes, discerning individual cell bodies for cell counting was not possible. Instead, the proportion of cortex occupied by reactive astrocytic signal (% GFAP signal) was determined by first setting a pixel intensity threshold to the mean pixel value of layer I/II–III, where the most intense signal was localized. Because the majority of pixels in a given image are not GFAP-signal, the pixels below the mean can be discounted as noise. Once thresholded, the GFAP signal was determined by automating a count of the non-zero pixels (n = 5). Implanted cortex and contralateral cortex were compared for all metrics by t-tests with significance level of $\alpha = 0.05$.

We identified cell-types in the encapsulation tissue based on morphology and antibody staining. Vimentin(+)/Iba-1(+) and vimentin(−)/Iba-1(+) cells were considered to be macrophages if found in the meninges or microglia if found in the parenchyma. Vimentin(+)/Iba-1(−) cells were considered to be fibroblasts. Multi-nucleated cells were considered cells that contained more than one Hoescht 33342 labeled nuclei in a single cell body. These cells are often found in pathological inflammatory conditions or in the presence of chronically implanted foreign bodies (Lynn et al., 2011; Brodbeck et al., 2002; Anderson et al., 2008).

2.7. Collagen-I imaging

Collagen I, a key component of tissue encapsulation, can be visualized using second-harmonic generation (SHG) imaging. SHG imaging takes advantage of a second-order nonlinear optical property of collagen type I to visualize an intrinsically-generated optical signal that can be used to locate and quantify collagen I in tissue. This is preferred to traditional histological staining protocols, which have been shown to have less signal specificity and require chemical processing that may alter the tissue quality (Strupler et al., 2007; Cox et al., 2003).

SHG images of tissue encapsulation and dura mater were captured using a laser with a Nikon A1Plus multiphoton scanning confocal microscope and Nikon NIS- Elements Microscope Imaging Software. SHG was generated at an 830nm wavelength, and signal was collected via a bandpass filter that isolated tissue auto-fluorescence (435 − 700nm) and a low-pass filter that isolated SHG signal (<492nm). Images were taken with a 25× objective to maximize signal resolution and imaging frame; stitching software (EIS-Elements Microscope Imaging Software, Nikon) was used to consolidate disconnected images to make a seamless, high-resolution image of the encapsulation through the dorsal-ventral plane.

Encapsulation and dura mater thickness were determined by measuring average thickness of tissue extent as denoted by auto-fluorescence. Because SHG signal was confined within an uninterrupted, fibrous area, percent SHG-signal was measured by dividing the average thickness of SHG area by the total tissue thickness. Such measures were generated for encapsulation tissue from the ventral and dorsal sites, as well as for control dura mater (n = 5 tissue sections for all groups). Encapsulation and dura mater thickness and percent SHG signal were compared between ventral encapsulation, dorsal encapsulation, and control dura mater groups by one-way ANOVA tests with Tukey's post-hoc tests. Significance for all comparisons was defined to be $\alpha = 0.05$.

3. Results

3.1. Cortical architecture

Upon sacrifice and explantation, we found that the ECoG grid was fully encapsulated in fibrous tissue that was contiguous with the dura mater (Figure 1F). The brain underneath the encapsulated ECoG grid was mechanically depressed. We assessed the extent of this depression by generating a 3D rendering of the brain's surface topography. Then, the image of the implanted hemisphere was superimposed onto the non-implanted hemisphere. This allowed us to quantify the topographic differences between the two hemispheres (Figure 1D). We found that the brain region under the ECoG grid was mechanically depressed by as much as 3.63 mm relative to the same region of the non-implanted hemisphere.

To determine if this gross morphological change resulted in alterations of cortical cytoarchitecture, we evaluated neuronal and glial density as well as cortical thickness under the grid. We compared these metrics of cortical structure to those of the corresponding cortex in the opposite hemisphere (Figure 2). The density of neurons labeled with the NeuN antibody in layers I/II–III or layer V was not significantly higher (Student's t-test, $p = 0.5$ and 0.32, respectively) in the cortex under the grid versus the contralateral cortex (Figure 2A). Similarly, the signal intensity of GFAP antibody labeling of reactive astrocytes in layers I/II–III or layer V was not significantly different between the two hemispheres (Figure 2B; 0.18 and 0.73, respectively). Only the density of microglia labeled with the Iba-1 antibody and located in the superficial layers (I/II–III) exhibited a significant increase under the array (Figure 3A; t-test $p = 0.027$ for layers I/II–III; 0.24 for layer V). The microglia both under the array and in the contralateral cortex exhibited a qualitatively similar morphology, with only cell density along the dorsal surface of the cortex of either hemisphere (7.6 ± 1.6 versus 6.6 ± 1.8 cells/mm for the implanted and control cortical surface, respectively) showing surface-directed morphology (defined in Methods) (Figure 3B). These cells typically had

processes polarized parallel to the cortical surface. Finally, the thickness of the Nissl-stained cortical tissue under the grid (Figure 2C, top; 2.8 ± 0.04mm) was not statistically different from that of the contralateral cortex (Figure 2C, bottom; 2.7 ± 0.09mm; t-test: $p = 0.34$). These findings were qualitatively corroborated by observing the transition region of tissue at the edge of the ECoG array and tissue immediately adjacent to the implanted region, where limited changes were observed (Supplemental Figure A1). Taken together, these tests provide evidence of little to no cytological changes in the cortex underlying the ECoG array.

3.2. Fibrous encapsulation

Chronic subdural ECoG implantation resulted in fibrous encapsulation of the grid. The grid was removed by making an incision along the anterior portion of the encapsulation and pulling the grid with forceps. Surprisingly, the grid offered little mechanical resistance to removal, indicating that adhesion between the grid and encapsulation tissue was minimal. Using second-harmonic generation (SHG) imaging, we detected collagen I in sections of both the tissue encapsulation and control dura mater (> 2cm from implantation site). Using filters to image second-harmonic signals and tissue autofluorescence simultaneously, we quantified both the thickness of encapsulation tissue and the percentage of encapsulation tissue that was collagen I-positive (Figure 4). Because the dorsal portion of the encapsulation emerged from the original, autografted dura mater, we analyzed it separately from the ventral portion of the encapsulation, which grew *de novo* following initial implantation. Both sides of the tissue encapsulation were compared to control dura mater taken more than 2cm from the implantation site. There were statistically significant differences in the thicknesses of the tissues (one-way ANOVA: $F(2, 14) = 136.13$, $p < 0.001$), with both dorsal encapsulation (0.82 ± 0.04mm) and ventral encapsulation (1.76 ± 0.09mm) being thicker than control dura mater (0.36 ± 0.03mm; Tukey's post-test: $p = 0.001$). The ventral encapsulation was also significantly thicker than dorsal encapsulation ($p < 0.001$). The encapsulation was presumably the major contributor to the visible depression of the cortex under the grid.

SHG imaging revealed encapsulation tissue to be comprised of a cellular region that did not express strong SHG signal and a collagenous region that was strongly SHG(+) (Figure 4B,E). Using the tissue thickness derived above, we were able to assess the relative proportions of cellular and collagenous regions by measuring the area of collagenous region (SHG(+) region) and dividing it by tissue thickness. This showed that the proportion of collagenous region was significantly different between the tissues (one-way ANOVA: $F(2, 14) = 44.33$; $p < 0.001$). Control dura mater had a significantly higher percentage of collagenous tissue (96.4 ± 0.33%) than either ventral encapsulation (82.5 ± 2.3%; Tukey's post-test: $p < 0.01$) or dorsal encapsulation (58.9 ± 4.5%; $p < 0.001$). The percentage of collagenous tissue in the ventral encapsulation was also significantly greater than that of the dorsal encapsulation ($p < 0.001$).

In order to determine the cellular composition of the encapsulation we used immunohistochemistry (described in section 2.5). We identified fibroblasts and macrophages in all tissue groups. Control dura mater was largely composed of fibroblasts, many of which exhibited elongated nuclei (Figure 5C), consistent with previous literature (Adeeb et al.,

2012). Macrophages were sparsely distributed. This resembled the "collagenous" region (>300μm from the array; Figure 5B) of the tissue encapsulation, which also contained elongated fibroblasts and macrophages. The "cellular" region of encapsulation (< 300μm from the array; Figure 5A) was highly cell dense with round, mononuclear macrophages as well as multinuclear, foreign body giant cells (vimentin(+)/Iba-1(+)). We made the mononuclear/multinuclear distinction based on nuclei count (Figure 5A *inset*). The encapsulation was organized as a gradient, with "cellular" tissue closest to the array exhibiting more inflammatory cell activity, and "collagenous" tissue more distal to the array more closely resembling healthy dura mater.

3.3. Physiological recordings

In order to validate long-term signal modulation, we examined ECoG signals during center-out reaching task trials conducted between day 542 and 562 post-implantation. Signals exhibited clear modulation with target direction (Figure 6, Supplemental Figures B1, B2). Characteristic decreases in the mu and beta frequency bands (10–30 Hz), in conjunction with increases in the high-gamma band (> 60 Hz), were observed. High-gamma band modulation was found to be the strongest over the 70 – 100 Hz frequency range, and was tightly locked to movement onset. Thirteen of the fifteen electrodes exhibited reach-modulated signals. Of the two electrodes not exhibiting reach-related activity, one was a reference (dura-facing) electrode and the other an electrically intact electrode that was not recording due to a failure in the cabling connecting the Cereport adapter and neural recording amplifier.

Prior to hand control experiments, a number of recording sessions devoted to BMI control experiments were conducted. However, during post-hoc analysis of these data we discovered that the animal had developed a strategy of using artifacts, possibly the result of jaw movement, to generate directionally-modulated broadband increases in spectral power. We now believe that our earlier report of stable multi-day BMI control was due in part to this strategy (Ashmore et al., 2012). The presence of these artifacts precludes further analysis of the brain control data, apart from a baseline confirmation of the stability and robustness of the ECoG recordings. We have demonstrated this with representative mean electrode root-mean speed (RMS) amplitude measurements of ECoG signals, which initially dropped, but stabilized by day 300 post-implant (Supplemental Figure C1C,D).

We also tracked mean 20Hz impedance of all functional electrode sites during some recording sessions from day 52–562 post-implant as well as after electrode grid explantation (Supplemental Section C). Impedance was relatively stable through this time frame, though it fluctuated following surgical interventions (Supplemental Figure C1A). Depending on the impedance measurement method, mean impedance of the grid dropped 6–36 kOhms following removal from the tissue encapsulation (Supplemental Figure C1B).

4. Discussion

4.1. Histological findings

We examined the foreign-body response to a subdural ECoG electrode grid nearly two years after implantation. There was fibrotic growth around the electrode grid, resulting in a

shallow mechanical depression of the cortex under the array. Despite this, the cellular characteristics of the cerebral cortex underneath the ECoG grid were consistent with that of the tissue of the contralateral hemisphere, where no grid had been placed. Most importantly, cortical thickness and neuronal density of the tissue under the array were statistically indistinguishable from the contralateral tissue, with no morphological differences apparent at any spatial scale. After accounting for discrepancies in methods, our measurements of thickness and neuronal density for both hemispheres agreed with those of previous anatomical studies of primate frontal cortex (Matelli et al., 1991; Gittins and Harrison, 2004). Noting that cortical thickness and layering was unaffected by the gross mechanical deformation of the brain's surface, it is plausible that the displaced brain was merely pushed into the ventricles, as is observed in cerebral edema and subdural hematoma (Kim and Gean, 2011). Only the microglial density of the superficial cortical layers was significantly different between the implanted and non-implanted hemispheres. It is possible that the persistent, unactivated microglia population was part of the foreign body response to the implanted ECoG array, where increased macrophage density persists in the vicinity of the implant for its lifetime (Anderson, 2001; Sanders et al., 2000). It is also conceivable that this activation was not in response to a foreign body, but rather from pervasive mechanical stress caused by the fibrous encapsulation compressing the brain (Roth et al., 2014; Ding et al., 2008). With the exception of a population of cells at the cortical surface of both hemispheres, layer I microglia were either ramified or polarized but without processes that extended to the cortical surface, indicating that these microglia were not actively responding to trauma or other noxious stimuli at the surface of the brain (Stence et al., 2001; Roth et al., 2014; Nimmerjahn et al., 2005; Kozai et al., 2012). The microglia at the surface of the brain were polarized with processes extending parallel to the cortical surface, similar to a cell type that has been described in healthy mouse cerebellum and rat prefrontal cortex, suggesting the observed cell type is not a result of pathology (Vela et al., 1995; Kongsui et al., 2014). The astrocytic GFAP expression between control and implanted hemispheres was not different. For both hemispheres, we observed low GFAP expression in the gray matter and relatively strong expression in the glia limitans. This expression pattern has been well documented in healthy macaque brain, with gray matter GFAP expression increasing only in response to trauma or chronic foreign body implantation (Eng et al., 2000; Griffith and Humphrey, 2006; Peters and Sethares, 2002). Qualitatively, our finding of low levels of gray-matter GFAP(+) cells under the array suggests that the array was not actively causing trauma to the cortex.

During the grid implantation surgery, we resected the dura mater, replaced it over the ECoG array, and sutured it in place. After the 666 days of implantation, dura mater/fibrous encapsulation tissue was found in a contiguous piece surrounding both the top and bottom of the ECoG. Since there were only leptomeninges separating the brain and array at the time of the implant, we assume that the ventral encapsulation grew *de novo* post-implantation. This is similar to recent findings by Schendel et al., who reported progressive fibrous overgrowth of epidural ECoG grids, with complete encapsulation as early as one month post-implantation (Schendel et al., 2014; Schendel et al., 2013). The cellular distribution in the dorsal and ventral tissue encapsulation was distinct from dura mater elsewhere in the brain, and implied that the wound-healing response to implantation consisted of a stereotypic

foreign body response, which involves aggregation of mononuclear macrophages and multinucleated foreign body giant cells to the implant site and encapsulation of the device in a collagenous envelope. Aggregated cells and tissue encapsulation generally persist through the lifetime of an implant, with pro-inflammatory cytokine expression diminishing within the first month as anti-inflammatory/pro-wound healing cytokines are expressed (Lynn et al., 2011; Brodbeck et al., 2002; Anderson et al., 2008). The fibrous encapsulation demarcates the final stage of wound healing in which the tissue disrupted by implantation is either regenerated from cells of the original cell type, or replaced with fibrous connective tissue. Given that dura mater is already largely fibrous connective tissue and mesenchymally derived fibroblasts, it was not clear to us the extent to which the tissue encapsulation was fibrous encapsulation or remodeled/regrown dura mater (Adeeb et al., 2012; Anderson, 2001; Anderson et al., 2008). We observed a gradient where tissue proximal to the implant more closely resembled fibrous encapsulation, and tissue distal to the implant more closely resembled control dura mater.

Both the dorsal encapsulation and ventral encapsulation were thicker than the control dura mater, which would be expected of a foreign body tissue encapsulation. In the case of autografted, dorsal encapsulation, dural thickening may have also been an inevitable consequence of craniotomy and/or durotomy that was simply exacerbated by the presence of a foreign body. This is seen in epidural ECoG implants, where encapsulation with ventral and/or dorsal dural thickening has been reported in long-term implants (Schendel et al., 2014). Merely performing a craniotomy triggered a 3.8 fold increase in dural thickness at 3 weeks, with a reduction to a 2.6 fold increase at 3 months in New Zealand white rabbits (Nunamaker and Kipke, 2010). Replacing dura with an alginate hydrogel resulted in a 2.8 fold increase of dural thickness of regrown dura at 3 weeks and a 3.1 fold increase at 3 months. Dural thickening of 2mm 8 weeks after a 2cm dural incision has also been observed in coonhound dogs; following application of a poly(ethylene) glycol based dural sealant, the healed dura was found to have thickened as much as 4mm (Preul et al., 2003). Meningeal cells almost double collagen production following subarachnoid hemorrhage in rats (Sajanti et al., 1999); computational models of collagen I fibrosis following biomaterial implantation corroborate this (Su et al., 2011). In these experiment-validated models, increasing numbers of fibroblasts at the implant site results in significantly increased collagen deposition. Since the predominating cell type of dura mater is the fibroblast, it is plausible that we might expect pronounced collagen I production following implantation.

Despite the degree of encapsulation, the ECoG grid was extracted from the fibrous tissue with little effort, indicating relatively minor adhesions between the encapsulation and device. This is not surprising given the lack of porosity and surface features on the silicone grid. Previous studies have demonstrated that smooth, non-porous dural substitutes are less susceptible to fibrosis and adhesion formation (Barbolt et al., 2001; Sayama et al., 2014).

While we have shown that the foreign body response to chronic ECoG grid implantation can result in grid encapsulation after approximately 22 months, we were unable to determine its exact time course. It is unclear whether the encapsulation was stable, still growing, or perhaps shrinking, at the time of electrode explantation. Subdural ECoG electrodes implanted up to 30 days clinically for epilepsy monitoring do not exhibit such encapsulation

(Fountas and Smith, 2007, Van Gompel et al., 2008, Wong et al., 2009, Wang et al., 2013), so it is likely that the subdural implant encaspulation response occurs on the order of months rather than weeks. Meningeal thickening without encapsulation has been observed in mirco-ECoG arrays in rats at 6 months post-implant, though no other time-points were assessed (Henle et al., 2011). In contrast, epidural implant encapsulation has been observed as soon as one month post-implant, with dramatically slower tissue encapsulation observed under an epidural array that had torn the dura mater during implantation (Schendel et al., 2014; Schendel et al., 2013). This suggests that there may be different foreign body response mechanisms for implants with different degrees of invasiveness. To our knowledge, there is no study directly comparing implantation depth to explore possible foreign body response mechanisms.

4.2. ECoG recording quality

ECoG electrodes provided recordings of physiological signals for nearly two years. Issues with the animal that were unrelated to the ECoG grid determined the termination date of the study, but we believe that signal quality may have persisted past two years. Of the fifteen electrodes on the array, only one lost recording capability during the course of our study. Post-explantation, we determined that failure was on account of a faulty wire connecting the Cereport adapter to the neural amplifier, and not due to the tissue response. We found that all functional electrodes showed signals that were temporally modulated and spatially tuned during a reaching task.

We conducted extensive BMI control tasks as part of this study. By the time we detected that the animal had developed a strategy of generating an electromyographic artifact (believed to be the result of jaw or face muscle contraction) to control the cursor, we were unable to train him to abandon this strategy. This made it difficult to study the functional properties of ECoG signals during the BMI control sessions. Despite the lack of longitudinal BCI performance data, both impedance and RMS amplitude measurements were relatively stable from day 56 (our earliest time-point measured) to day 562 post-implantation. The stable impedance and RMS amplitude suggest that the encapsulation did not significantly compromise the device functionality. However, future studies using a stereotypical experimental paradigm, such as the center-out task, will likely be able to better characterize changes in ECoG signal properties throughout the entire lifespan of an ECoG implant.

4.3. Implications and future directions

We believe our results have implications for the viability of ECoG for long-term high-resolution brain recording. In addition to its use as a recording modality for brain-machine interfaces, ECoG has increasingly become a neuroimaging method of choice in a variety of neuroscience fields and non-BMI neural recording and neuromodulation applications. The potential for subdural ECoG grids to remain implanted for extended periods of time without damaging the cortex could facilitate the study of cognitive processes over long timescales. Lack of cortical damage combined with the ease of removal of the ECoG grid from encapsulation tissue may provide the possibility for re-implantation in case of device failure. This is not practical for intracortical electrodes, which typically damage neural tissue upon insertion (Barrese et al., 2013). While ECoG grid encapsulation presents as a potentially

detrimental consequence of implantation, many strategies can and have been pursued to minimize the foreign body response. These include altering the shape of array substrate (Schendel et al., 2014; Schendel et al., 2013; Yamakwa et al., 2010), increasing array flexibility (Kim et al., 2010; Yeager et al., 2008; Rubehn et al., 2009), applying anti-fouling or biomimetic surface treatments (Collier et al., 2004; Kolarcik et al., 2012), and releasing anti-inflammatory drugs from the array substrate or electrodes (Norton et al., 2005; Weaver et al., 2014). Use of such strategies may help to further increase the stability of long-term ECoG recordings by eliminating changes in recording quality resulting from the foreign body response to subdural ECoG grids.

As the presented work constitutes a case study of long-term grid implantation in a single animal, future studies are required to fully assess the impact of chronically-implanted ECoG electrodes. Nevertheless, our findings of meningeal thickening, encapsulation, and fibrosis echo studies on subdural and epidural implants in rats (Henle et al., 2011; Schendel et al., 2013; Schendel et al., 2014) as well as in long-term (> 1 year) subdural and epidural implants in humans (Nashold and Friedman, 1972; Pineda, 1978; Saitoh et al., 2000; Sillay et al., 2013). There are fewer studies on the health of neural tissue underlying these implants. Additionally, we believe that our results provide an analytical framework for further investigation into the effects of chronic implantation of ECoG electrodes on the health of cortical tissue.

This study is an important first step toward fully assessing the long-term use of chronically-implanted ECoG electrode grids. Minimal cortical tissue damage from chronic electrode implantation suggests that ECoG may provide the capability to record physiological signals from the cortex for extended periods of time. Ultimately, this highlights the utility of ECoG as a valuable tool for long-term BMI, clinical, and neuroscientific studies.

Supplementary Material

Refer to Web version on PubMed Central for supplementary material.

Acknowledgments

The authors would like to thank Dr. Jason Godlove and Melissa Faulkner for their help in training the animal used in this study; Dr. Douglas Weber and Erin Gaia for their assistance in the explantation surgery; Darina Sipula and the Systems Neuroscience Institute for their assistance in the histological analysis; Dr. Simon Watkins, Dr. Gregory Gibson, and the Center for Biological Imaging for their assistance in SHG and confocal imaging; and Dr. J. Andrew Holmes and the Swanson Center for Product Innovation for their assistance in 3D scanning. The work was supported by NIH Grants R01NS062019, 3R01NS050256-05S1, R01 NS065065, R01 RHD071686A, KL2TR000146, and P30 NS076405. The work was also supported by the National Science Foundation, the Burroughs Wellcome Fund, the UPMC Rehabilitation Institute, and the Craig H. Neilsen Foundation. The content is solely the responsibility of the authors and does not necessarily represent the official views of the National Institutes of Health.

References

Acharya S, Fifer MS, Benz HL, Crone NE, Thakor NV. Electrocorticographic amplitude predicts finger positions during slow grasping motions of the hand. Journal of Neural Engineering. 2010; 7(4):046002. [PubMed: 20489239]

Adeeb N, Mortazavi MM, Tubbs RS, Cohen-Gadol AA. The cranial dura mater: a review of its history, embryology, and anatomy. Child's Nervous System. 2012; 28(6):827–837.

Anderson JM. Biological Response to Materials. Annual Review of Materials Research. 2001; 31:81–100.

Anderson JM, Rodriguez A, Chang DT. Foreign Body Reaction to Biomaterials. Seminars in Immunology. 2008; 20(2):86–100. [PubMed: 18162407]

Ashmore R, Endler B, Smalianchuk I, Degenhart A, Hatsopoulos N, Tyler-Kabara E, Batista A, Wang W. Stable Online Control of an Electrocorticographic Brain-Computer Interface Using a Static Decoder. Conf Proc IEEE Eng Med Biol Soc. 2012; 2012:1740–1744. [PubMed: 23366246]

Ball T, Schulze-Bonhage A, Aertsen A, Mehring C. Differential representation of arm movement direction in relation to cortical anatomy and function. Journal of Neural Engineering. 2009; 6(1): 016006. [PubMed: 19155551]

Barbolt TA, Odin M, Léger M, Kangas L, Holste J, Liu SH. Biocompatibility evaluation of dura mater substitutes in an animal model. Neurological Research. 2001; 23(8):813–820. [PubMed: 11760872]

Barrese JC, Rao N, Paroo K, Triebwasser C, Vargas-Irwin C, Franquemont L, Donoghue JP. Failure mode analysis of silicon-based intracortical microelectrode arrays in non-human primates. Journal of Neural Engineering. 2013; 10(6):066014. [PubMed: 24216311]

Biran R, Martin DC, Tresco PA. Neuronal cell loss accompanies the brain tissue response to chronically implanted silicon microelectrode arrays. Experimental Neurology. 2005; 195(1):115–126. [PubMed: 16045910]

Biran R, Martin DC, Tresco PA. The brain tissue response to implanted silicon microelectrode arrays is increased when the device is tethered to the skull. Journal of biomedical materials research. Part A. 2007; 28(1):169–178. [PubMed: 17266019]

Bjornsson CS, Oh SJ, Al-Kofahi YA, Lim YJ, Smith KL, Turner JN, De S, Roysam B, Shain W, Kim SJ. Effects of insertion conditions on tissue strain and vascular damage during neuroprosthetic device insertion. Journal of Neural Engineering. 2006; 3(3):196–207. [PubMed: 16921203]

Bouchard KE, Mesgarani N, Johnson K, Chang EF. Functional organization of human sensorimotor cortex for speech articulation. Nature. 2013; 495:327–332. [PubMed: 23426266]

Cervenka MC, Boatman-Reich DF, Ward J, Franaszczuk PJ, Crone NE. Language mapping in multilingual patients: electrocorticography and cortical stimulation during naming. Frontiers in Human Neuroscience. 2011; 22(5):13. [PubMed: 21373361]

Chao ZC, Nagasaka Y, Fujii N. Long-term asynchronous decoding of arm motion using electrocorticographic signals in monkeys. Frontiers in Neuroengineering. 2010; 3:3. [PubMed: 20407639]

Chestek CA, Gilja V, Blabe CH, Foster BL, Shenoy KV, Parvizi J, Henderson JM. Hand posture classification using electrocorticography signals in the gamma band over human sensorimotor brain areas. Journal of Neural Engineering. 2013; 10(2):026002. [PubMed: 23369953]

Chestek CA, Gilja V, Nuyujukian P, Foster JD, Fan JM, Kaufman MT, Churchland MM, Rivera-Alvidrez Z, Cunningham JP, Ryu SI, Shenoy KV. Long-term stability of neural prosthetic control signals from silicon cortical arrays in rhesus macaque motor cortex. Journal of Neural Engineering. 2011; 8(4):045005. [PubMed: 21775782]

Collier TO, Anderson JM, Brodbeck WG, Barber T, Healy KE. Inhibition of macrophage development and foreign body giant cell formation by hydrophilic interpenetrating polymer network. Journal of Biomedical Materials Research Part A. 2004; 69(4):644–650. [PubMed: 15162406]

Collinger JL, Wodlinger B, Downey JE, Wang W, Tyler-Kabara EC, Weber DJ, McMorland AJ, Velliste M, Boninger ML, Schwartz AB. High-performance neuroprosthetic control by an individual with tetraplegia. Lancet. 2012; 381:507–598.

Cox G, Kable E, Jones A, Fraser I, Manconi F, Gorrell MD. 3-Dimensional imaging of collagen using second harmonic generation. Journal of Structural Biology. 2003; 141(1):53–62. [PubMed: 12576020]

Crone NE, Hao L, Hart J, Boatman D, Lesser RP, Irizarry R, Gordon B. Electrocorticographic gamma activity during word production in spoken and sign language. Neurology. 2001; 57(11):2045–2053. [PubMed: 11739824]

Degenhart, AD.; Collinger, JL.; Vinjamuri, R.; Kelly, J.; Tyler-Kabara, EC.; Wang, W. Classification of hand posture from electrocorticographic signals recorded during varying force conditions;

Engineering in Medicine and Biology Society, EMBC, 2011 Annual International Conference of the IEEE; 2011a.

Degenhart AD, Kelly JW, Ashmore RC, Collinger JL, Tyler-Kabara EC, Weber DJ, Wang W. Craniux: A LabVIEW-Based Modular Software Framework for Brain-Machine Interface Research. Computational Intelligence and Neuroscience. 2011b; 2011:363565. [PubMed: 21687575]

Ding MC, Lo EH, Stanley GB. Sustained focal cortical compression reduces electrically induced seizure threshold. Neuroscience. 2008; 154(2):551–555. [PubMed: 18495350]

Edwards E, Soltani M, Deouell LY, Berger MS, Knight RT. High gamma activity in response to deviant auditory stimuli recorded directly from human cortex. Journal of Neurophysiology. 2005; 94(6): 4269–4280. [PubMed: 16093343]

Eng LF, Ghirnikar RS, Lee YL. Glial fibrillary acidic protein: GFAP-thirty-one years (1969–2000). Neurochemical research. 2000; 25(9–10):1439–1451. [PubMed: 11059815]

Flint RD, Wright ZA, Scheid MR, Slutzky MW. Long term, stable brain machine interface performance using local field potentials and multiunit spikes. Journal of Neural Engineering. 2013; 10(5):056005. [PubMed: 23918061]

Fountas KN, Smith JR. Subdural Electrode-Associated Complications: A 20-Year Experience. Stereotactic and functional neurosurgery. 2007; 85(6):264–272. [PubMed: 17709978]

Freire MAM, Morya E, Faber J, Santos JR, Guimaraes JS, Lemos NA, Sameshima K, Pereira A, Ribeiro S, Nicolelis MA. Comprehensive analysis of tissue preservation and recording quality from chronic multielectrode implants. PLoS ONE. 2011

Ganguly K, Carmena JM. Emergence of a stable cortical map for neuroprosthetic control. PLoS Biology. 2009; 6(11):e27554.

Gittins R, Harrison PJ. Neuronal density, size and shape in the human anterior cingulate cortex: a comparison of Nissl and NeuN staining. Brain Research Bulletin. 2004; 63(2):155–160. [PubMed: 15130705]

Griffith GW, Humphrey DR. Long-term gliosis around chronically implanted platinum electrodes in the *Rhesus macaque* motor cortex. Neuroscience Letters. 2006; 406:81–86. [PubMed: 16905255]

Henle C, Raab M, Cordeiro JG, Doostkam S, Schulze-Bonhage A, Stieglitz T, Rickert J. First long term in vivo study on subdurally implanted micro-ECoG electrodes, manufactured with a novel laser technology. Biomedical microdevices. 2011; 13(1):59–68. [PubMed: 20838900]

Hotson G, McMullen DP, Fifer MS, Johannes MS, Katyal KD, Para MP, et al. Individual finger control of a modular prosthetic limb using high-density electrocorticography in a human subject. Journal of Neural Engineering. 2016; 13(2):026017. [PubMed: 26863276]

Jung J, Mainy N, Kahane P, Minotti L, Hoffmann D, Bertrand O, Lachaux J-P. The neural bases of attentive reading. Human brain mapping. 2008; 29(10):1193–1206. [PubMed: 17894399]

Kellis S, Miller K, Thomson K, Brown R, House P, Greger B. Decoding spoken words using local field potentials recorded from the cortical surface. Journal of Neural Engineering. 2010; 7:056007. [PubMed: 20811093]

Kelly JW, Siewiorek DP, Smailagic A, Wang W. Automated filtering of common-mode artifacts in multichannel physiological recordings. IEEE transactions on bio-medical engineering. 2013; 60(10):2760–2770. [PubMed: 23708770]

Kim JJ, Gean AD. Imaging for the diagnosis and management of traumatic brain injury. Neurotherapeutics: The Journal of the American Society for Experimental NeuroTherapeutics. 2011; 8:39–53. [PubMed: 21274684]

Kim DH, Viventi J, Amsden JJ, Xiao J, Vigeland L, Kim YS, Blanco JA, Panilatis B, Frechette ES, Contreras D, Kaplan DL, Omenetto FG, Huang Y, Hwang KC, Zakin MR, Litt B, Rogers JA. Dissolvable films of silk fibroin for ultrathin conformal bio-integrated electronics. Nature Materials. 2010; 9:511–517. [PubMed: 20400953]

Kolarcik CL, Bourbeau D, Azemi E, Rost E, Zhang L, Lagenaur CF, Weber DJ, Cui XT. In vivo effects of L1 coating on inflammation and neuronal health at the electrode/tissue interface in rat dorsal root ganglion and spinal cord. Acta Biomaterialia. 2012; 8(10):3561–3575. [PubMed: 22750248]

Konsui R, Beynon SB, Johnson SJ, Walker FR. Quantitative assessment of microglial morphology and density reveals remarkable consistency in the distribution and morphology of cells within the

healthy prefrontal cortex of the rat. Journal of Neuroinflammation. 2014; 11:182. [PubMed: 25343964]

Kozai TDY, Vasquez AL, Weaver CL, Kim S-G, Cui XT. *In vivo* two-photon microscopy reveals immediate microglial reaction to implantation of microelectrode through extension of processes. Journal of Neural Engineering. 2012; 9:066001. [PubMed: 23075490]

Kubanek J, Miller KJ, Ojemann JG, Wolpaw JR, Schalk G. Decoding flexion of individual fingers using electrocorticographic signals in humans. Journal of Neural Engineering. 2009; 6(6):066001. [PubMed: 19794237]

Lachaux J-P, George N, Tallon-Baudry C, Martinerie J, Hugueville L, Minotti L, Kahane P, Renault B. The many faces of the gamma band response to complex visual stimuli. NeuroImage. 2005; 25:491–501. [PubMed: 15784428]

Leuthardt EC, Gaona C, Sharma M, Szrama N, Roland J, Freudenberg Z, Solis J, Breshears J, Schalk G. Using the electrocorticographic speech network to control a brain-computer interface in humans. Journal of Neural Engineering. 2011; 8:036004. [PubMed: 21471638]

Leuthardt EC, Schalk G, Moran D, Ojemann JG. The emerging world of motor neuroprosthetics: a neurosurgical perspective. Neurosurgery. 2006; 59:1–14. [PubMed: 16823294]

Leuthardt EC, Schalk G, Wolpaw JR, Ojemann JG, Moran DW. A brain-computer interface using electrocorticographic signals in humans. Journal of Neural Engineering. 2004; 1(2):63–71. [PubMed: 15876624]

Lynn AD, Blakney AK, Kyriakides TR, Bryant SJ. Temporal progression of the host response to implanted poly(ethylene glycol)-based hydrogels. Journal of Biomedical Materials Research Part A. 2010; 96(4):621–631. [PubMed: 21268236]

Mainy N, Kahane P, Minotti L, Hoffmann D, Bertrand O, Lachaux J-P. Neural correlates of consolidation in working memory. Human brain mapping. 2007; 28(3):183–193. [PubMed: 16767775]

Matelli M, Luppino G, Rizzolatti G. Architecture of superior and mesial area 6 and the adjacent cingulate cortex in the macaque monkey. The Journal of Comparative Neurology. 1991; 311(4): 445–462. [PubMed: 1757597]

McConnell GC, Rees HD, Levey AI, Gutekunst C-A, Gross RE, Bellamkonda RV. Implanted neural electrodes cause chronic, local inflammation that is correlated with local neurodegeneration. Journal of Neural Engineering. 2009; 6(5):056003. [PubMed: 19700815]

Miller KJ, Zanos S, Fetz EE, Den Nijs M, Ojemann JG. Decoupling the Cortical Power Spectrum Reveals Real-Time Representation of Individual Finger Movements in Humans. Journal of Neuroscience. 2009; 29(1):3132–3137. [PubMed: 19279250]

Moran D. Evolution of brain-computer interface: action potentials, local field potentials and electrocorticograms. Current opinion in neurobiology. 2010; 20(6):741–745. [PubMed: 20952183]

Morrell MJ. RNS System in Epilepsy Study Group. Responsive cortical stimulation for the treatment of medically intractable partial epilepsy. Neurology. 2011; 77(13):1295–1304. [PubMed: 21917777]

Nakanishi Y, Yanagisawa T, Shin D, Fukuma R, Chen C, Kambara H, Yoshimura N, Hirata M, Yoshimine T, Koike Y. Prediction of Three-Dimensional Arm Trajectories Based on ECoG Signals Recorded from Human Sensorimotor Cortex. PLoS ONE. 2013; 8(8):e72085. [PubMed: 23991046]

Nashold BS, Friedman H. Dorsal column stimulation for control of pain: Preliminary report on 30 patients. Journal of Neurosurgery. 1972; 36:490–497. [PubMed: 5013621]

Nimmerjahn A, Kirchhoff F, Helmchen F. Resting microglial cells are highly dynamic surveillants of brain parenchyma in vivo. Science. 2005; 308:1314–1318. [PubMed: 15831717]

Norton LW, Tegnell E, Toporek SS, Reichert WM. In vitro characterization of vascular endothelial growth factor and dexamethasone releasing hydrogels for implantable probe coatings. Biomaterials. 2005; 26(16):3285–3297. [PubMed: 15603824]

Nunamaker EA, Kipke DR. An alginate hydrogel dura mater replacement for use with intracortical electrodes. Journal of biomedical materials research. 2010; 95(2):421–429. [PubMed: 20878928]

Pasley BN, David SV, Mesgarani N, Flinker A, Shamma SA, Crone NE, Knight RT, Chang EF. Reconstructing speech from human auditory cortex. PLoS Biology. 2012; 10(1):e1001251. [PubMed: 22303281]

Pei X, Barbour DL, Leuthardt EC, Schalk G. Decoding vowels and consonants in spoken and imagined words using electrocorticographic signals in humans. Journal of Neural Engineering. 2011; 8(4): 046028. [PubMed: 21750369]

Peters A, Sethares S. The effects of age on the cells in layer 1 of primate cerebral cortex. Cerebral Cortex. 2002; 12:27–36. [PubMed: 11734530]

Pineda A. Complications of dorsal column stimulation. Journal of Neurosurgery. 1978; 48:64–68. [PubMed: 304096]

Pistohl T, Ball T, Schulze-Bonhage A, Aertsen A, Mehring C. Prediction of arm movement trajectories from ECoG-recordings in humans. Journal of Neuroscience Methods. 2008; 167(1):105–114. [PubMed: 18022247]

Polikov VS, Tresco PA, Reichert WM. Response of brain tissue to chronically implanted neural electrodes. Journal of Neuroscience Methods. 2005; 148(1):1–18. [PubMed: 16198003]

Preibisch S, Saalfeld S, Tomancak P. Globally optimal stitching of tiled 3D microscopic image acquisitions. Bioinformatics. 2009; 25(11):1463–1465. [PubMed: 19346324]

Preul MC, Bichard WD, Spetzler RF. Toward optimal tissue sealants for neurosurgery: use of a novel hydrogel sealant in a canine durotomy repair model. Neurosurgery. 2003; 53(5):1189–1198. [PubMed: 14580287]

Ray S, Niebur E, Hsiao SS, Sinai A, Crone NE. High-frequency gamma activity (80–150Hz) is increased in human cortex during selective attention. Clinical neurophysiology: official journal of the International Federation of Clinical Neurophysiology. 2008; 119(1):116–133. [PubMed: 18037343]

Roth TL, Nayak D, Atanasijevic T, Koretsky AP, Latour LL, McGavern DB. Transcranial amelioration of inflammation and cell death after brain injury. Nature. 2014; 505:223–228. [PubMed: 24317693]

Rousche PJ, Normann RA. Chronic recording capability of the Utah Intracortical Electrode Array in cat sensory cortex. Journal of Neuroscience Methods. 1998; 82(1):1–15. [PubMed: 10223510]

Rubehn B, Bosman C, Oostenveld R, Fries P, Stieglitz T. A MEMS-based flexible multichannel ECoG-electrode array. Journal of Neural Engineering. 2009; 6(3):036003. [PubMed: 19436080]

Saitoh Y, Shibata M, Hirano S-I, Hirata M, Mashimo T, Yoshimine T. Motor cortex stimulation for central and peripheral deafferentation pain: Report of eight cases. Journal of Neurosurgery. 2000; 92:150–155. [PubMed: 10616094]

Sanders JE, Stiles CE, Hayes CL. Tissue response to single-polymer fibers of varying diameters: evaluation of fibrous encapsulation and macrophage density. Journal of Biomedical Materials Research. 2000; 52(1):231–237. [PubMed: 10906696]

Sajanti J, Bjorkstrand A-S, Finnila S, Heikkinen E, Peltonen J, Majamaa K. Increase of collagen synthesis and deposition in the arachnoid and the dura following subarachnoid hemorrhage in the rat. Biochimica et Biophysica Acta. 1999; 1454(3):209–216. [PubMed: 10452955]

Sayama CM, Sorour M, Schmidt RH. Dural adhesion to porous cranioplastic implant: A potential safety concern. Surgical Neurology International. 2014; 5:19. [PubMed: 24778907]

Schalk G, Miller KJ, Anderson NR, Wilson JA, Smyth MD, Ojemann JG, Moran DW, Wolpaw JR, Leuthardt EC. Two-dimensional movement control using electrocorticographic signals in humans. Journal of Neural Engineering. 2008; 5(1):75–84. [PubMed: 18310813]

Schalk G, Lethardt EC. Brain-computer interfaces using electrocorticographic signals. IEEE Reviews in Biomedical Engineering. 2011; 4:140–154. [PubMed: 22273796]

Schendel AA, Nonte MW, Vokoun C, Richner TJ, Brodnick SK, Atry F, Frye S, Bostrom P, Pashale R, Thongpang S, Eliceirl KW, Williams JC. The effect of micro-ECoG substrate footprint on the meningeal tissue response. Journal of Neural Engineering. 2014; 11(4):046011. [PubMed: 24941335]

Schendel AA, Thongpang S, Brodnick SK, Richner TJ, Lindevig BDB, Krugner-Higby L, Williams JC. A cranial window imaging method for monitoring vascular growth around chronically

implanted micro-ECoG devices. Journal of Neuroscience Methods. 2013; 218(1):121–130. [PubMed: 23769960]

Schwartz AB. Cortical neural prosthetics. Annual Review of Neuroscience. 2004; 27:487–507.

Schwartz AB, Cui XT, Weber DJ, Moran DW. Brain-controlled interfaces: movement restoration with neural prosthetics. Neuron. 2006; 52(1):205–220. [PubMed: 17015237]

Saxena T, Karumbaiah L, Gaupp EA, Patkar R, Patil K, Betancur M, Stanley GB, Bellamkonda RV. The impact of chronic blood-brain barrier breach on intracortical electrode function. Biomaterials. 2013; 34(20):4703–4713. [PubMed: 23562053]

Shimoda K, Nagasaka Y, Chao ZC, Fujii N. Decoding continuous three-dimensional hand trajectories from epidural electrocorticographic signals in Japanese macaques. Journal of Neural Engineering. 2012; 9(3):036015. [PubMed: 22627008]

Sillay KA, Rutecki P, Cicora K, Worrell G, Drazkowski J, Shih JJ, Sharan AD, Morrell MJ, Williams J, Wingeier B. Long-Term Measurement of Impedance in Chornically Implanted Depth and Subdural Electrodes During Responsive Neurostimulation in Humans. Brain Stimulation. 2013; 6:718–726. [PubMed: 23538208]

Simeral JD, Kim S-P, Black MJ, Donoghue JP, Hochberg LR. Neural control of cursor trajectory and click by a human with tetraplegia 1000 days after implant of an intracortical microelectrode array. Journal of Neural Engineering. 2011; 8(2):025027. [PubMed: 21436513]

Slutzky MW, Jordan LR, Krieg T, Chen M, Mogul DJ, Miller LE. Optimal spacing of surface electrode arrays for brain-machine interface applications. Journal of Neural Engineering. 2010; 7(2):26004. [PubMed: 20197598]

Stence N, Waite M, Dailey ME. Dynamics of microglial activation: A confocal time-lapse analysis in hippocampal slices. Glia. 2001; 33(3):256–266. [PubMed: 11241743]

Strupler M, Pena AM, Hernest M, Tharaux PL, Martin JL, Beaurepaire E, Schanne-Klein MC. Second harmonic imaging and scoring of collagen in fibrotic tissues. Optics Express. 2007; 15(7):4054–4065. [PubMed: 19532649]

Su J, Todorov M, Gonzales HP, Perkins L, Kojouharov H, Weng H, Tang L. A Predictive Tool for Foreign Body Fibrotic Reactions Using 2-Dimensional Computational Model. Open access bioinformatics. 2011; 3:19–35. [PubMed: 21836814]

Szarowski DH, Andersen MD, Retterer S, Spence AJ, Isaacson M, Craighead HG, Turner JN, Shain W. Brain responses to micro-machined silicon devices. Brain research. 2003; 938(1–2):23–35. [PubMed: 12914963]

Tallon-Baudry C, Bertrand O, Hénaff M-A, Isnard J, Fischer C. Attention modulates gamma-band oscillations differently in the human lateral occipital cortex and fusiform gyrus. Cerebral cortex. 2005; 15(5):654–662. [PubMed: 15371290]

Trautner P, Rosburg T, Dietl T, Fell J, Korzyukov OA, Kurthen M, Schaller C, Elger CE, Boutros NN. Sensory gating of auditory evoked and induced gamma band activity in intracranial recordings. NeuroImage. 2006; 32(2):790–798. [PubMed: 16809054]

Turner JN, Shain W, Szarowski DH, Andersen M, Martins S, Isaacson M, Craighead H. Cerebral astrocyte response to micromachined silicon implants. Experimental neurology. 1999; 156(1):33–49. [PubMed: 10192775]

Van Gompel JJ, Worrell GA, Bell ML, Patrick TA, Cascino GD, Raffel C, Marsh WR, Meyer FB. Intracranial electroencephalography with subdural grid electrodes: techniques, complications, and outcomes. Neurosurgery. 2008; 63(3):498–505. [PubMed: 18812961]

Vela JM, Dalmau I, Gonzalez B, Castellano B. Morphology and distribution of microglial cells in the young and adult mouse cerebellum. The Journal of Comparative Neurology. 1995; 361:602–616. [PubMed: 8576417]

Wang W, Collinger JL, Degenhart AD, Tyler-Kabara EC, Schwartz AB, Moran DW, Weber DJ, Wodlinger B, Vinjamuri RK, Ashmore RC, Kelly JW, Boninger ML. An electrocorticographic brain interface in an individual with tetraplegia. PLoS ONE. 2013; 8(2):e55344. [PubMed: 23405137]

Wang W, Degenhart AD, Collinger JL, Vinjamuri R, Sudre GP, Adelson PD, Holder DL, Leuthardt EC, Moran DW, Boninger ML, Schwartz AB, Crammond DJ, Tyler-Kabara EC, Weber DJ. Human motor cortical activity recorded with Micro-ECoG electrodes, during individual finger movements.

Conference proceedings: Annual International Conference of the IEEE Engineering in Medicine and Biology Society IEEE Engineering in Medicine and Biology Society Conference. 2009; 2009:586–589.

Wang W, Degenhart AD, Sudre GP, Pomerleau D, Tyler-Kabara EC. Decoding semantic information from human electrocorticographic (ECoG) signals. Engineering in Medicine and Biology Society, EMBC, 2011 Annual International Conference of the IEEE. 2011; 2011:6294–6298.

Wang Y, Papadimitrakopoulos F, Burgess DJ. Polymeric "smart" coatings prevent foreign body response to implantable biosensors. Journal of Controlled Release. 2013; 169(3):341–347. [PubMed: 23298616]

Weaver CL, LaRosa JM, Luo X, Cui XT. Electrically Controlled Drug Delivery from Graphene Oxide Nanocomposite Films. ACS Nano. 2014; 8(2):1834–1843. [PubMed: 24428340]

Wilson JA, Felton EA, Garell PC, Schalk G, Williams JC. ECoG factors underlying multimodal control of a brain-computer interface. IEEE transactions on neural systems and rehabilitation engineering: a publication of the IEEE Engineering in Medicine and Biology Society. 2006; 14(2):246–250.

Wolpaw JR, Birbaumer N, McFarland DJ, Pfurtscheller G, Vaughan TM. Brain-computer interfaces for communication and control. Clinical neurophysiology: official journal of the International Federation of Clinical Neurophysiology. 2002; 113(6):767–791. [PubMed: 12048038]

Wong CH, Birkett J, Byth K, Dexter M, Somerville E, Gill D, Chaseling R, Fearnside M, Bleasel A. Risk factors for complications during intracranial electrode recording in presurgical evaluation of drug resistant partial epilepsy. Acta Neurochirurgica. 2009; 151(1):37–50. [PubMed: 19129963]

Xu HT, Pan F, Yang G, Gan WB. Choice of cranial window type for *in vivo* imaging affects dendritic spine turnover in the cortex. Nature Neuroscience. 2007; 10:549–551. [PubMed: 17417634]

Yamakawa T, Yamakwa T, Aou S, Ishizuka S, Suzuki M, Fujii M. Subdural electrode array manipulated by a shape memory allow guidewire for minimally-invasive electrocorticogram recording. World Automation Congress. 2010

Yanagisawa T, Hirata M, Saitoh Y, Kishima H, Matsushita K, Goto T, Fukuma R, Yokoi H, Kamitani Y, Yoshimine T. Electrocorticographic control of a prosthetic arm in paralyzed patients. Annals of Neurology. 2012; 71(3):353–361. [PubMed: 22052728]

Yeager JD, Phillips DJ, Rector DM, Bahr DF. Characterization of flexible ECoG electrode arrays for chronic recording in awake rats. Journal of Neuroscience Methods. 2008; 173(2):279–285. [PubMed: 18640155]

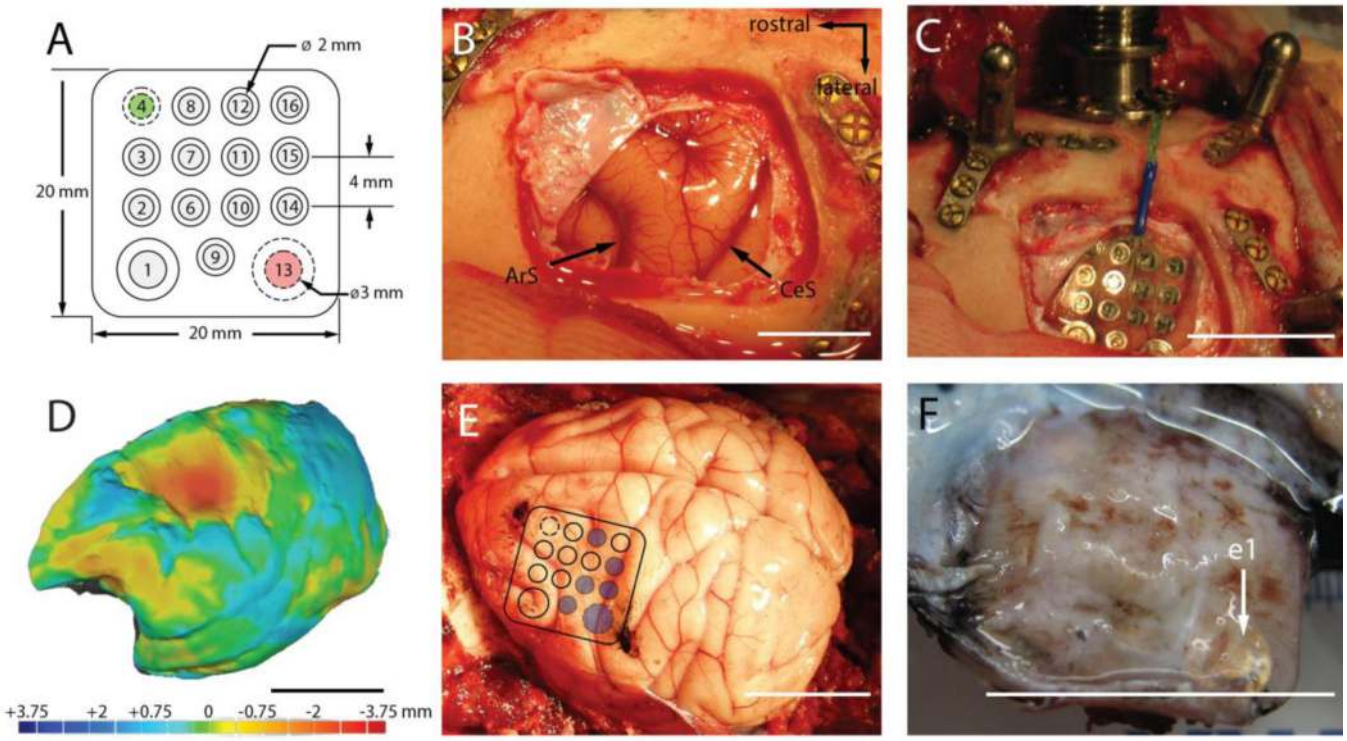

Figure 1.

(A). Top view of the electrode grid. The neural recording electrodes (gray) face the cortical surface. The reference (#4, green) and ground (#13, red) electrodes face the dura. (B). Exposure of the left motor cortex prior to implantation (ArS: arcuate sulcus, CeS: central sulcus). (C). Placement of the electrode grid. (D). 3D rendering of the left-hemisphere superimposed on the mirror image of the right-hemisphere. Heat map denotes difference in surface topography between hemispheres in mm. (E). ECoG grid location superimposed on the postmortem brain. Blue circles indicate electrode sites targeted for histological analysis. Black ink marks the observed location of the rostral-medial and caudal-lateral corners of the grid. (F). Underside of the encapsulated grid following explantation. The location of electrode 1 (e1) is indicated by the white arrow. All scale bars are approximately 2cm unless otherwise indicated.

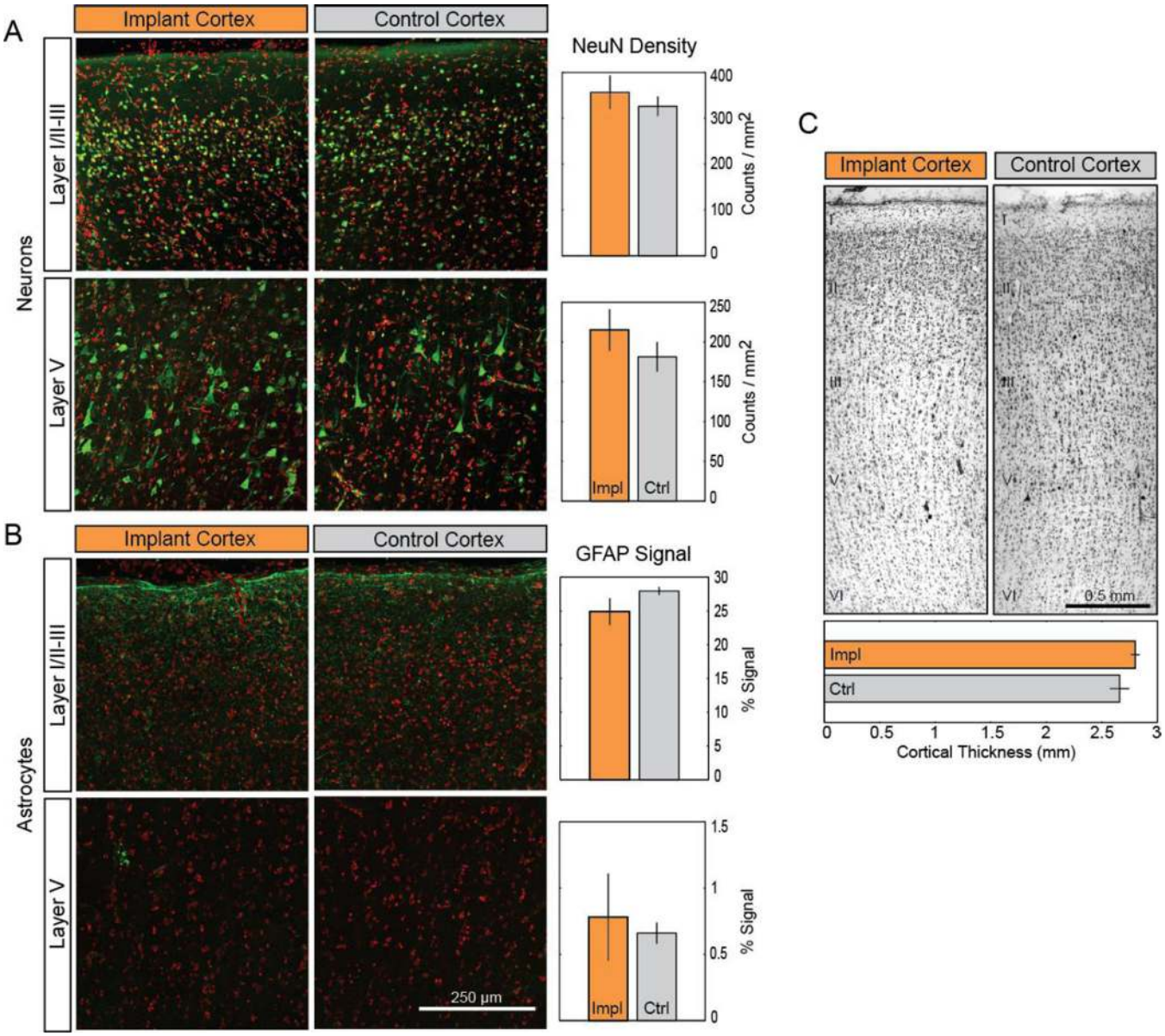

Figure 2.

Long-term ECoG grid implantation causes minimal changes in cortical cytoarchitecture. (A–B). Neither the density of NeuN-labeled neurons (A; green) nor the signal intensity of GFAP-labeling in astrocytes (B; green) located in layers I/II–III or layer V were significantly affected by implantation. Cell nuclei (red) counterstained with Hoescht 33342. Data presented as mean ± SEM; * denotes significant difference from control ($p < 0.05$). (C). Comparison of Nissl-stained motor cortex between implanted and control hemispheres. Cortical layers are indicated by roman numerals I– VI. *Impl*: implanted cortex. *Ctl*: control cortex.

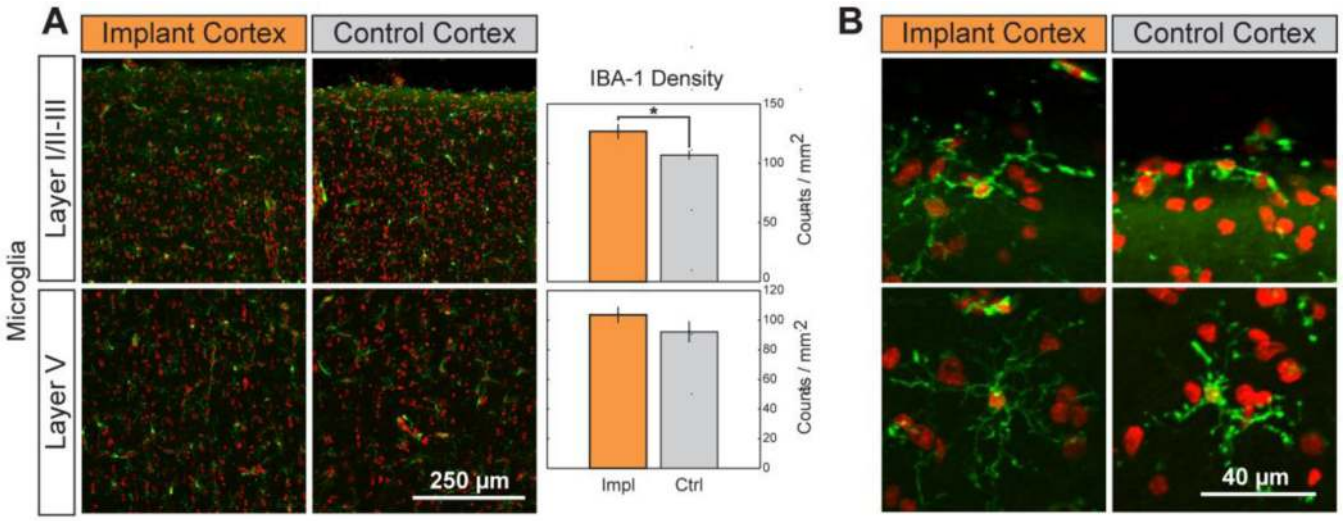

Figure 3.

Chronic implantation yields higher microglial density with no change in cell morphology. (A). The density of microglia (green; nuclei in red) was significantly increased in layers I/II–III but not in layer V following implantation. Data presented as mean ± SEM; * denotes significant difference from control ($P < 0.05$). (B). Layer I microglia show no morphological indication of inflammatory response. A small population at the cortical surface of implant and control cortices are polarized along the curvature of the brain, all microglia beneath the surface are unresponsive.

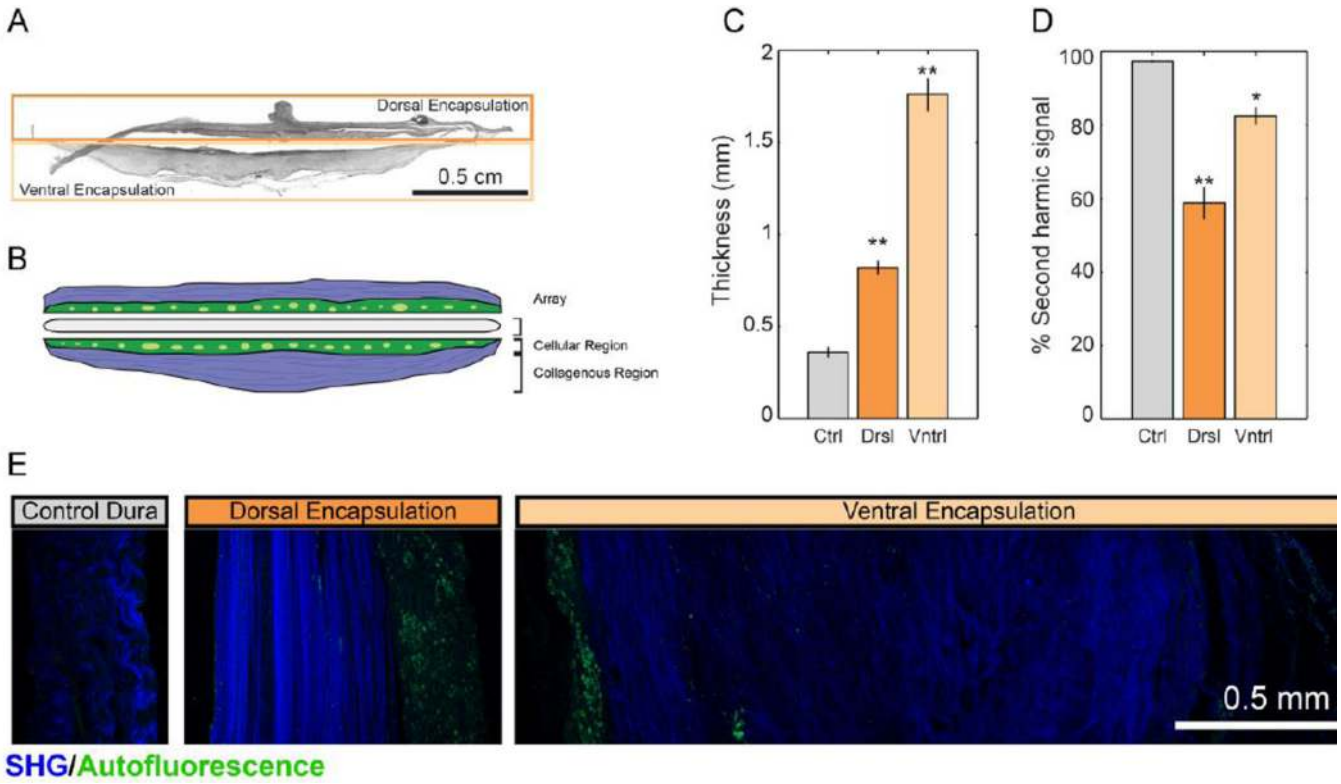

Figure 4.

Second-harmonic imaging of fibrous encapsulation reveals fibrous, cell-sparse regions and cell-dense regions in both dorsal and ventral aspects of encapsulation. (A). Sample image of full tissue encapsulation slice. (B) Schematic representation of encapsulation components. (C). Comparison of thickness of dorsal and ventral aspects of encapsulation tissue to control dura. (D). Percentage of SHG(+) tissue was significantly reduced in encapsulation tissue. (E). Sample images of dorsal encapsulation, central encapsulation, and control dura with SHG signal shown in blue and tissue autofluorescence shown in green. Data presented as mean ± SEM. Asterisks * and ** denote significant differences from control at $p < 0.01$ and $p < 0.001$, respectively.

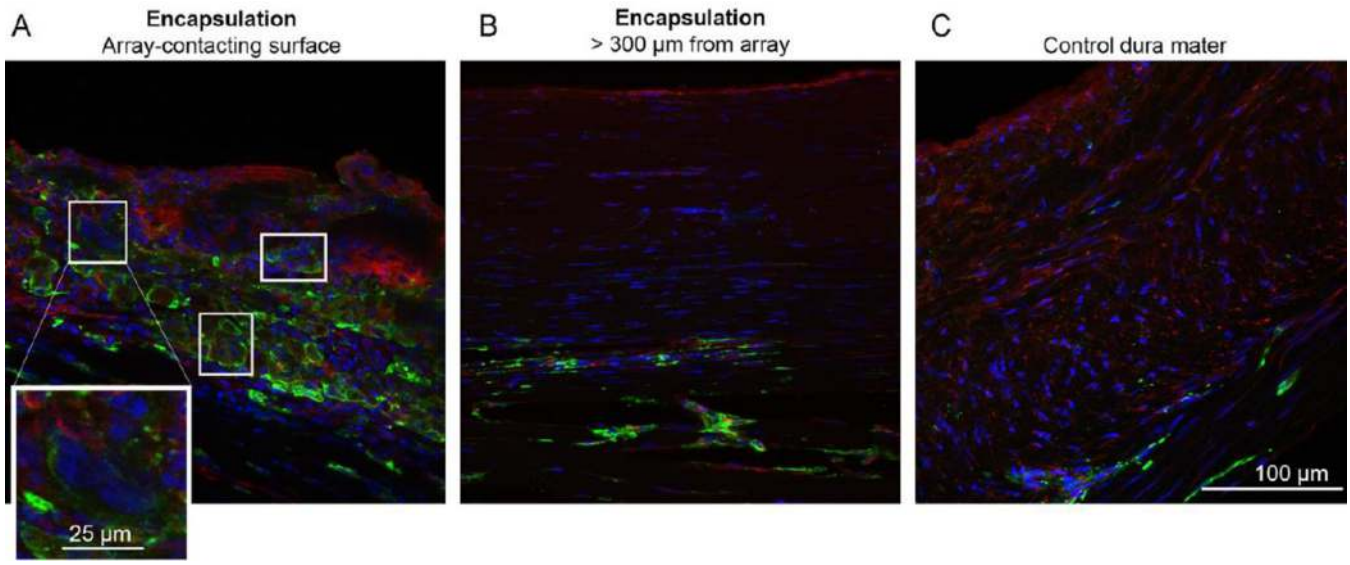

Figure 5.

Immunohistochemical staining of encapsulation tissue. Tissue was stained for nuclei (blue; Hoescht 33342) and antibodies directed to macrophages (green; Iba-1) or macrophages/ fibroblasts (red; vimentin). (A). Array-contacting aspects of the encapsulation were highly cell dense, populated with macrophages (vimentin(+ or −)/ Iba-1(+)) as well as fibroblasts (vimentin(+)/Iba-1(−)). Boxes indicate multinucleated giant cells. *Inset*: Magnification of a multi-nucleated giant cell. (B). Distal portions of encapsulation were hallmarked by elongated fibroblasts and macrophages (vimentin(−)/Iba-1(+)). (C). Control dura mater is largely composed of elongated fibroblasts with infrequent macrophages.

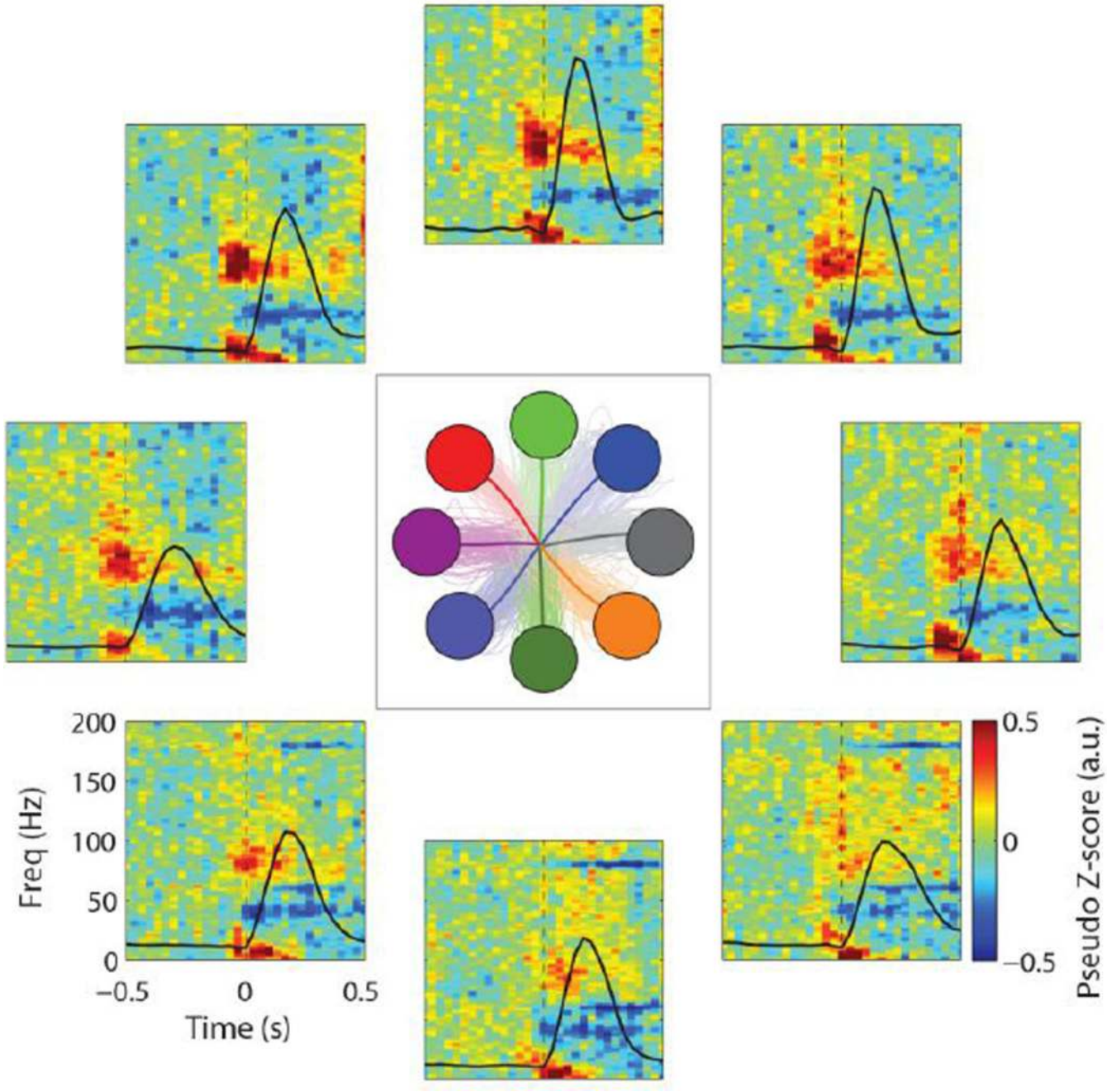

Figure 6.

ECoG signal modulation during 8-target center-out reach tasks. Average time-frequency data are shown for a single electrode (e10) for all reach directions. Averaged (thick lines) and individual trajectories (thin lines) for each target are shown in the center panel. Time-frequency data were normalized with respect to the spectral data during a central hold period preceding each trial. Black lines show average speed profiles for each target.